Surface Pressure Prediction for Bio-Inspired Unidirectional Canopies in Wall-jet Boundary Layers

Nandita Nurani Hari[1], Máté Szőke[2] and William J. Devenport,[3]
Center of Research in Experimental Aero/hydrodynamic Technology (CREATe), Department of Aerospace and Ocean Engineering, Virginia Tech, Blacksburg, VA 2406, USA

Stewart Glegg[4]
Department of Ocean and Mechanical Engineering, Florida Atlantic University, Boca Raton, FL 33431, USA

An analytical approach has been developed to model the rapid term contribution to the unsteady surface pressure fluctuations in wall jet turbulent boundary layer flows. The formulation is based on solving Poisson's equation for the turbulent wall pressure by integrating the source terms (Kraichnan, 1956). The inputs for the model are obtained from 2D time-resolved Particle Image Velocimetry measurements performed in a wall jet flow. The wall normal turbulence wavenumber two-point cross-spectra is determined using an extension of the von Kármán homogeneous turbulence spectrum. The model is applied to compare and understand the baseline flow in the wall jet and to study the attenuation in surface pressure fluctuations by unidirectional canopies (Gonzales *et al,* 2019). Different lengthscale formulations are tested and we observe that the wall jet flow boundary layer contributes to the surface pressure fluctuations from two distinct regions. The high frequency spectrum is captured well. However, the low frequency range of the spectrum is not entirely captured. This is because we have used PIV data only up to a height of 2.3δ, whereas the largest turbulent lengthscales in the wall jet are on the order of $y_{1/2} \approx 6\delta$. Using the flow data obtained from PIV and Pitot probe measurements, the model predicts a reduction in the surface pressure due to canopy at low frequencies.

I. Introduction

Mitigation of surface pressure fluctuations induced by boundary layer flows in applications such as wind turbines and aircraft trailing edges is crucial. These fluctuations also drive panel vibrations causing cabin noise and interior wind noise in cars. They also contaminate measurements made with surface-mounted instrumentation. On an atmospheric scale, surface pressure fluctuations are directly related to wind gust magnitude that can cause damage to structures. With the expansion in aviation industry, there is an increased attention towards noise reduction technologies of aircraft. Therefore, control of wall-bounded turbulent boundary layer flows is both technologically desirable and an interacting scientific problem in different aero-hydrodynamic applications.

Based on findings of Lilley (1998), flow noise generated from turbulent flow over aerodynamic surfaces could be reduced by manipulating the boundary layer itself. This phenomenon of shielding the surface by manipulating the flow and therefore the unsteady pressure fluctuations experiences is termed as Pressure shielding. This study is motivated by recent works beginning with Clark *et al* (2014) on bio-inspired surface treatments based on Owls' downy coating. They used canopies made using parallel array of streamwise fibers with an open-area ratio of 70% which showed promising reduction in the surface pressure fluctuations. The experiments were conducted in the Virginia Tech Anechoic Wall facility with fibers placed at nearly 40% of the boundary layer thickness from the wall. They found the attenuation increased exponentially with frequency and depended on the flow velocity. Cross-fibers in fabric canopies which were also tested shows significant self-noise. Practical application of unidirectional canopies requires reduction in wall pressure fluctuations without increasing the susceptibility of a boundary layer to separation or incurring too great an increase in the drag penalty. This work was extended to 'finlets' and 'rails' designed by modifying unidirectional canopies which were mounted on a DU96-W180 airfoil trailing edge (Clark *et al,* 2017). They observed suppression of surface pressure fluctuations and up to 10dB reduction in far-field noise between 2-5kHz in the treated locations for some cases. Subsequent studies conducted by Afshari *et al* (2017) and Millican *et al*

[1] Graduate Research Assistant.
[2] Senior Research Associate
[3] Professor, Associate Fellow AIAA.
[4] Professor, Associate Fellow AIAA.

(2017) attempted to understand the modification in the flow-field by finlets. Formation of shear layer and reduction in the mean velocity was observed for all treatments compared to the baseline flat-plate case. The turbulent kinetic energy profile also showed significant changes when compared to untreated case. The variations in both the flow quantities increased by increasing the finlet height and reducing the spacing between adjacent fins. The turbulent energy was observed to reduce near the wall and showed increased turbulence at the treatment height. Large-eddy simulations performed by Bodling *et al* (2019) on NACA 0012 airfoil with and without finlets showed that there was no significant difference in the aerodynamic performance of the airfoil in both cases. The simulations also showed lift-up of turbulence from the surface to the height of the finlets as observed in prior experiments.

Wall pressure fluctuations, as we see, play a crucial role in various applications to induce flow noise, disturbances to the surface signals, structural vibrations and so on. The accurate estimation of the wall pressure in many of these applications has been a challenge for decades, experimentally and otherwise. Experimental investigations by Willmarth (1956) and Bull (1967) laid the foundations of surface pressure measurement and advancement in the study of transducer size optimum for resolving the significant turbulent boundary layer scales. Studies on understanding the wall pressure scaling for a conventional turbulent boundary layer by Farabee and Casarella (1991) showed that the surface pressure had an outer and inner region of scaling. The outer region parameters are used to collapse the spectrum at low frequencies while the high frequency range scales on inner variables. Computational simulations starting with Reynolds Averaged Navier Stokes (RANS) models and Large Eddy Simulation (LES) models give information about the mean and the larger scales of the flow respectively and can be used to build predictive models towards estimating the surface pressure spectrum. In recent times, Direct Numerical Simulations (DNS) of the turbulent boundary layer provides the statistical information of the flow and wall pressure fluctuations as well. However, using DNS for real-time applications is not a computationally feasible option and therefore, we must rely on models to estimate the surface pressure fluctuations. Using such models also aids calculation of noise prediction from turbulent flow over surfaces. One of the fundamental works in this field was performed by Corcos (1964), who developed a mathematical equation based on curve-fitting various wall pressure data for flow conditions normalized on boundary layer parameters. Chase (1980) and Goody (2004) developed mathematical models to account for both low and high frequencies and the latter also included the Reynolds number effect. The first development of an analytical model to predict the surface pressure fluctuations in a turbulent boundary layer flow was developed by Kraichnan (1956).

This model was based on solving the Poisson's equation governing the turbulent wall pressure fluctuations. Further studies improved the flow models by incorporating semi-empirical models to predict the mean and statistical distributions of the boundary layer parameters (Panton and Linebarger, 1998). Recent studies by Slama *et al.* (2018) and Grasso *et al.* (2019) study the effect of mean flow interactions and turbulence interactions on the wall pressure spectra. Many of these models assume homogeneous and isotropic flow to predict the turbulent correlations and therefore it is often required to use corrections for accounting for inhomogeneity and anisotropy in the flow.

The purpose of this work is to develop a model for the surface pressure spectrum based on the linear source term in the Poisson's equation for the wall pressure using flow data provided from the 2D-Time Resolved-Particle Image Velocitmetry(TR-PIV) measurements. We have limited our study for this paper to using only the rapid source term. The model will be further used to predict the surface pressure data in the presence of unidirectional canopies.(Hari *et al*, 2021) and to understand the contributions of different flow terms in reducing the surface pressure fluctuations.

II. Experimental Setup

This study follows the previous works by Gonzalez *et al* (2019) and Hari *et al* (2021) on reduction of surface pressure fluctuations due to idealized, unidirectional rod canopies. The canopies were tested in the anechoic wall jet facility at Virginia Tech for jet flow speeds 20-50 m/s.

Canopy Geometry

The canopy treatments used in this study consist of evenly spaced array of rods placed streamwise to recreate the essential features of unidirectional canopies tested by Clark *et al.* (2014) as shown in Fig 1. Rods were chosen over previously used fibers because they can be cantilevered from downstream thereby eliminating influence of a leading edge structure. Spacing, s is defined as the distance between the mid-points of two consecutive rods. The height, h is measured from the bottom surface of the rods to the wall. The open area ratio given by $(s-d)/s$ is a crucial parameter

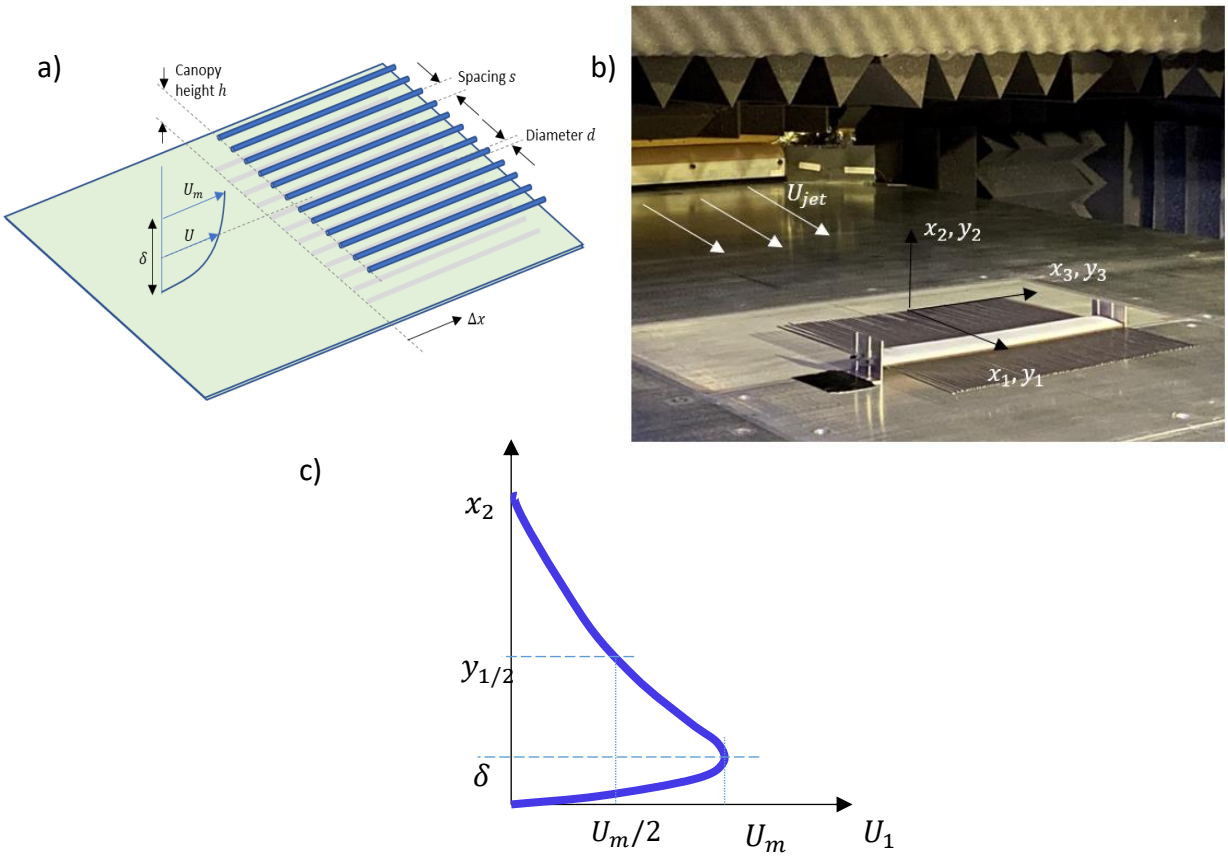

Figure 1a): Schematic of the unidirectional canopies showing the geometric parameters, when placed in a turbulent boundary layer flow(Gonzalez *et al*, 2019) b) Picture of the canopy place in the wall jet flow. x_1, y_1 represents the streamwise flow direction, x_2, y_2 is the wall normal direction and x_3, y_3 in the spanwise direction following the right-hand rule. The origin is mid-span, on the wall at the canopy leading edge location. C) Typical wall jet profile as a function of the wall normal distance showing the important parameters

used to characterize the canopy, where d is the rod diameter. The airfoil supporting the rods from downstream is designed to be aerodynamic to ensure minimal disturbance to the flow. The chord length of the airfoil, 25.4mm, is limited to avoid the large deflections of the rods at higher wall jet velocities. A McMasters Henderson airfoil was chosen for its structural rigidity and to minimize its self-noise. For this study, we have compared our model with the experimental results of Canopy D, which has a rod diameter of 2mm and spacing of 6mm and placed at a height, h of 6mm (Hari *et al*,2019). In this case the rods extend 305 mm upstream of the airfoil leading edge, and have the form of blunt cylinders at their upstream ends.

Apparatus and Instrumentation

The experiments were conducted in the Anechoic wall jet facility at Virginia Tech [Kleinfelter, 2019] for jet velocities ranging from 20-50m/s. The canopy leading edge was placed in the test-section with the leading edge at a distance of 1.28m from the nozzle exit, where the mean flow is spanwise uniform over a distance of some 490mm. The fully developed boundary layer in the test-section attains self-similarity and can be expressed using wall jet relations proposed by Wygnanski *et al*(2000).

A typical wall jet mean velocity profile and that of a canonical zero-pressure gradient turbulent boundary layer profile is shown in Fig. 1c The wall jet has an inner region extending from the wall to the boundary layer height, where the mean velocity attains a maximum. Beyond the boundary layer height, the velocity starts decreasing as the flow mixes with the quiescent air above thus forming an additional mixing or outer layer which is not observed in the canonical boundary layer. The wall jet flow is characterized by boundary layer thickness, δ, maximum boundary layer velocity, U_m and wall normal distance where the velocity is half of the maximum boundary layer velocity, $y_{1/2}$. Flow properties at the leading edge of the canopy are listed in table 1 for the baseline (no canopy) and Canopy D cases at a streamwise distance, x of 101.4 mm from canopy leading edge location.

Table 1: Boundary layer properties for the wall jet flow with and without the canopy for a jet velocity, U_j of 50m/s. The friction velocity, u_τ and skin-friction coefficient, C_f was estimated using walljet relations given by George et al(2000). Properties for Canopy D, with rod diameter, d of 2mm and spacing, s of 6mm at height, h of 6mm has been given here.

	Baseline	**Canopy**
δ	0.0132m	0.0164m
U_m	14.63m/s	14.55m/s
$y_{1/2}$	0.116m	0.118m
δ^*	7.5e-4m	16e-4m
θ	6.3e-4m	13e-4m
u_τ	0.7831 m/s	0.7639 m/s
C_f	0.0057	0.0055

Figure 1b shows the coordinate system, originating at the spanwise center of the canopy leading edge. Streamwise and spanwise array of Knowles (FG-23329-P07) surface pressure microphones are mounted on the wall underneath the canopy to measure the unsteady pressure. Data from the microphones was acquired using a six-channel Bruel and Kjaer Type 3050 24-bit LAN-XI modules. Post-processing was done using Fast Fourier Transform of the data sampled at 65536 Hz of record length of 8192 multiplied by a 50% overlap Hanning window. Figure 2 shows the schematic of streamwise microphone array locations underneath the canopy facing the incoming turbulent boundary layer. The legend shows the maximum velocity attained in the wall jet boundary layer at the canopy leading edge location for flow velocities ranging from 20-70m/s. The uncertainty in the jet velocity is $\pm$ 0.1 m/s.

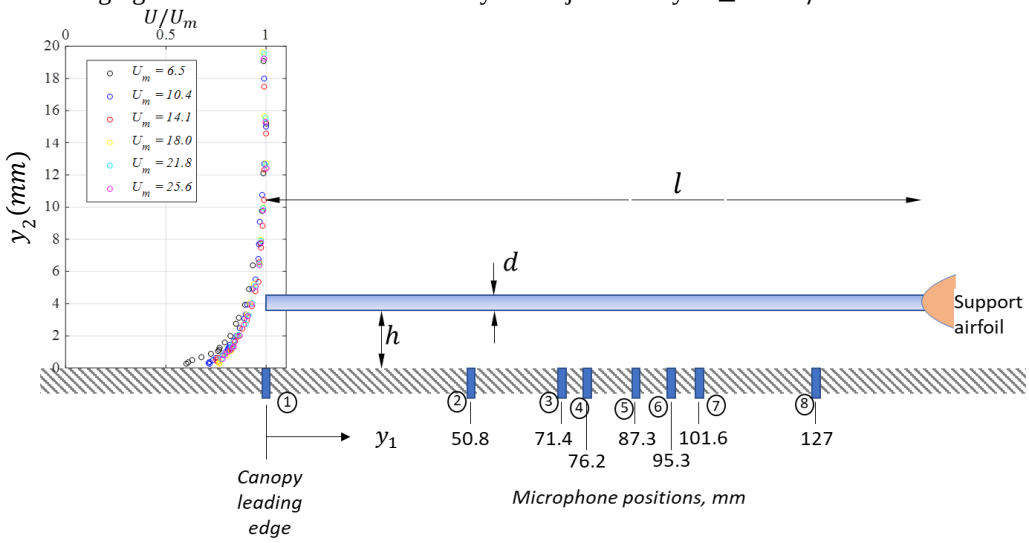

Figure 2 Schematic showing the surface microphone locations in the streamwise direction below the canopy. The legend represents the maximum boundary layer velocity for five jet velocities 20-70m/s.(Gonzalez *et al*, 2019)

A two-dimensional two-component high-speed PIV system (Fig 3a) is used to obtain the mean and the turbulent flow profiles in the wall-normal plane. A Photonics DM150-532 high-speed nanosecond laser and a LaVision high-speed controller generate the laser sheet to illuminate the seed particles, which are captured using a Phantom v2512 high-speed camera with 300mm/F4 Nikon lens and aperture of F5.6. Seeding of particles of size 0.5-0.7 μm were introduced using a MDG MAX300APS type fog generator. The field of view (FOV) was 80x50 mm and the data was processed using DaVis 10 software package. A 64x64 pix window with 50% overlap and 16x16 pix second window with 75% was used for processing to obtain a resolution of 0.25mm. The data was captured at two sampling rates, 1024 and 10240 frame pairs per second to obtain a fine spatial and temporal resolution respectively. This study uses data

obtained from the wall-normal FOV plane, i.e., velocity components in the streamwise and the wall-normal directions. While processing images with the canopy, the highly reflective area in the image was masked out to avoid errors from creeping into the results. Also, the data has been streamwise averaged between streamwise distances of 36mm and 116mm measured from the canopy leading edge.

A flat-head Pitot probe designed in-house (Clark *et al*, 2014) was used for the mean velocity measurements particularly between the canopy rods (Fig 3b). The measuring area of the probe is $0.082mm^2$ and the nearest wall distance that can be measured is 0.15mm. The probe holder was designed such that it could be traversed in the wall normal direction and also provision to make minor adjustments so that it could be placed very close to the surfaces. Data was measured using a Setra 239 pressure transducer, for eight seconds with a sampling rate of 6400 Hz and the mean velocity was calculated by averaging 50 records.

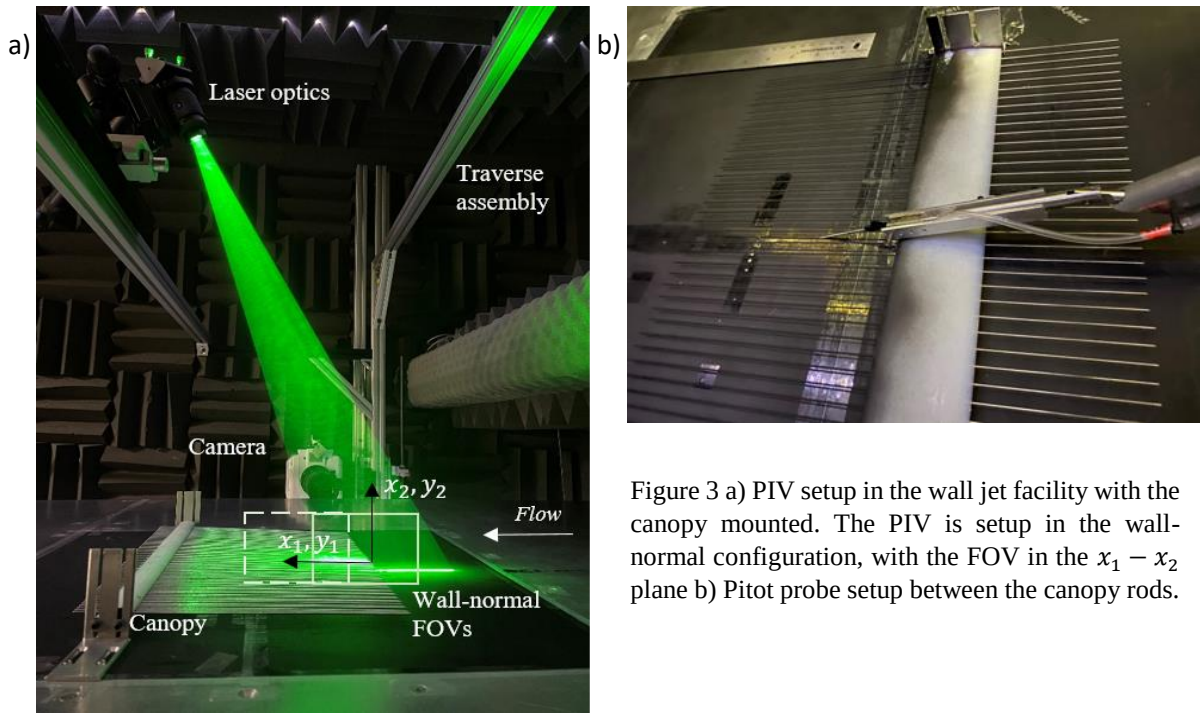

Figure 3 a) PIV setup in the wall jet facility with the canopy mounted. The PIV is setup in the wall-normal configuration, with the FOV in the $x_1 - x_2$ plane b) Pitot probe setup between the canopy rods.

III. Theoretical Modeling

The Poisson's equation for the wall pressure fluctuations in a turbulent boundary layer flow can be obtained starting from the general equation of momentum and taking its divergence [Glegg and Devenport, 2017]. Another way to derive is to apply the Curle's theorem to predict the pressure fluctuation produced by flow over a plane wall [Blake, 2017]. We can then use Reynolds decomposition to split the velocity, u_i into its mean represented as U_i or $\overline{u_i}$ and fluctuating parts, u_i' and subtract the time-averaged equation. For an incompressible, two-dimensional flow, the Pressure Poisson equation for the wall pressure is given by,

$$-\frac{1}{\rho}\nabla^2 p(\boldsymbol{x},t) = 2\frac{\partial U_1}{\partial x_2}\frac{\partial u'_2}{\partial x_1} + \frac{\partial^2}{\partial x_i \partial x_j}\left(u'_i u'_j - \overline{u'_i u'_j}\right) = q(\boldsymbol{x},t) \tag{3.1}$$

where $i,j = 1,2,3$ and $\boldsymbol{x} \equiv \{x_1, x_2, x_3\}$. The Laplacian of the wall pressure field is thus predominantly controlled by $q(\boldsymbol{x},t)$ which is a sum of two source terms. The first source is the mean gradient term or the rapid term, because it directly relates the changes in the mean flow velocity to the change in surface pressure fluctuations. This term represents the interaction between the mean shear and the turbulence in the flow. The second term represents the effect of turbulence-turbulence interactions on the wall pressure. This term is considered to be the slow or the non-linear term since it is an indirect consequence of the change in the mean velocity affecting the change in the flow turbulence. Earlier studies starting with Kraichnan, 1956 assume the rapid term to be dominant in boundary layers, however, recent DNS computations [Chang *et al*(1999), Grasso *et al*(2019)] show that both the source terms contributions are of the same order of magnitude.

Rapid term modeling

Our primary objective as we mentioned for the paper is to establish a model for the linear term. The wall pressure Poisson's equation with the rapid term is given by,

$$\nabla^2 p(\boldsymbol{x},t) = -2\rho \frac{\partial U_1}{\partial x_2}\frac{\partial u'_2}{\partial x_1} = q(\boldsymbol{x},t) \tag{3.2}$$

One way to solve this is to Fourier transform the equation to frequency- wavenumber space. Typically, for a turbulent boundary layer flow with mean gradient in the wall-normal direction, it is fair to assume homogenous flow in the streamwise, x_1 and spanwise x_3 directions, but not in the x_2 direction. Based on this, the inverse Fourier transform for $q(\boldsymbol{x},t)$ can be written as,

$$q(\boldsymbol{x},t) = \iiint_{-\infty}^{\infty} \hat{q}(k_1,k_3,x_2,\omega) e^{-i\omega t + ik_1x_1 + ik_3x_3} d\omega dk_1 dk_3 \tag{3.3}$$

Where k_1 and k_3 are the streamwise and spanwise wavenumbers, and ω is the angular frequency. The resultant pressure field based on this source formulation, can also be represented in a similar form,

$$p(\boldsymbol{x},t) = \iiint_{-\infty}^{\infty} \hat{p}(k_1,k_3,x_2,\omega) e^{-i\omega t + ik_1x_1 + ik_3x_3} d\omega dk_1 dk_3 \tag{3.4}$$

Replacing the left and right sides of Eq 3.2 with Eqs 3.3 and 3.4, we obtain integral equations with the same variables and limits of integration. Equating the integrands on both sides, the Poisson's equation in the frequency-wavenumber domain is given by,

$$\frac{\partial^2 \hat{p}(k_1,k_3,x_2,\omega)}{\partial x_2^2} - (k_1^2 + k_3^2)\hat{p}(k_1,k_3,x_2,\omega) = \hat{q}(k_1,k_3,x_2,\omega) \tag{3.5}$$

Noting that $k = \sqrt{k_1^2 + k_3^2}$ considering waves parallel to the surface and assuming an implicit dependency on the frequency, ω, the above equation can be solved using variable separable technique [Grasso *et al* (2019)] to give,

$$\hat{p}(k_1,k_3,x_2 = 0,\omega) = \int_0^{R\infty} \frac{e^{-ky_2}}{k} \hat{q}(k_1,k_3,y_2,\omega) dy_2 \tag{3.6}$$

This method introduces an independent coordinate, $\boldsymbol{y}$, representing the domain of integration. In our case, the coordinate $\boldsymbol{y}$ is associated with location of the source. R_∞ is the limit of $\boldsymbol{y}$ integration, i.e. represents the extent of the domain. Expanding the source term and mentioning the dependencies of the velocity terms, Eq 3.6 can be written as,

$$\hat{p}(k_1,k_3,x_2 = 0,\omega) = \int_0^{R\infty} -2\rho \frac{\partial U_1(y_2)}{\partial y_2}\left(ik_1\hat{u}_2(k_1,k_3,y_2,\omega)\right)\frac{e^{-ky_2}}{k} dy_2 . \tag{3.7}$$

The wavenumber-frequency spectra of the wall pressure can be obtained as $\frac{\pi}{TR_\infty^2} E[\hat{p}(k_1,k_3,\omega)\hat{p}^*(k_1',k_3',\omega)] = \Phi_{pp}(k_1,k_3,\omega)$. Therefore, multiplying Eq 3.7 with its conjugate and taking the ensemble average, we obtain the wall pressure spectrum as a function of k_1, k_3 and ω.

$$\Phi_{pp}(k_1,k_3,\omega) = \frac{\pi}{TR_\infty^2}\left[4\rho_o^2 \int_0^{\infty}\int_0^{\infty} \frac{k_1^2}{k^2}\frac{\partial U_1(y_2)}{\partial y_2}\frac{\partial U_1(y_2')}{\partial y_2} E[\hat{u}_2(k_1,k_3,y_2,\omega)\hat{u}_2(k_1,k_3,y_2',\omega)] e^{-k(y_2+y_2')} dy_2 dy_2'\right] \tag{3.8}$$

Similarly, the ensemble average of the vertical velocity fluctuations at y_2 and y_2' can be written as the wavenumber frequency of the wall normal velocity cross-spectrum, $\frac{\pi}{TR_\infty^2} E[\hat{u}_2(k_1,k_3,y_2,\omega)\hat{u}_2(k_1,k_3,y_2',\omega)] =$

$\phi_{22}(k_1, k_3, y_2, y_2', \omega)$. The resultant spectrum for an incompressible, two-dimensional, turbulent boundary layer flow is given as,

$$\Phi_{pp}(k_1, k_3, \omega) = 4\rho_o^2 \int_0^\infty \int_0^\infty \frac{k_1^2}{k^2} \frac{\partial U_1(y_2)}{\partial y_2} \frac{\partial U_1(y_2')}{\partial y_2} \phi_{22}(k_1, k_3, y_2, y_2', \omega) e^{-k(y_2+y_2')} dy_2 dy_2' \tag{3.9}$$

Turbulence modeling

There are primarily two flow quantities required out of which the mean velocity is relatively easier to obtain for a variety of flow cases. For our study, the mean velocity is obtained directly from the PIV measurement. The primary challenge faced here is the modeling of wall normal turbulence spectrum, ϕ_{22}, which is difficult to obtain experimentally. The turbulence spectrum can be represented in its normalized form $\bar{\phi}_{22}$ as,

$$\phi_{22}(k_1, k_3, y_2, y_2', \omega) = \sqrt{\overline{u_2'^2}(y_2)\overline{u_2'^2}(y_2')}\,\bar{\phi}_{22}(k_1, k_3, y_2, y_2', \omega) \tag{3.10}$$

Blake (2017) simplifies the turbulence model assuming Taylor's hypothesis, connecting the frequency and wavenumber domains, using a separable form by incorporating the moving axis spectrum, $\phi_{22}(\vec{k}, \omega) = \phi_{22}(\vec{k})\phi_m(\omega - \vec{U}_{conv}.\vec{k})$. $\vec{U}_{conv}$ can be assumed to be the mean velocity at which the turbulent structures are being convected given by $U_{conv} \approx \omega/k_1$. We can consider the local convection velocity to be parallel to the streamwise direction and additionally choosing a delta function for ϕ_m consistent with Taylor's frozen convection hypothesis with a convection velocity U_{conv} gives,

$$\phi_{pp}(k_1, k_3, \omega) = 4\rho_o^2 \int_0^\infty \int_0^\infty \frac{k_1^2}{k^2} \frac{\partial U_1(y_2)}{\partial y_2} \frac{\partial U_1(y_2')}{\partial y_2} \sqrt{\overline{u_2'^2}(y_2)\overline{u_2'^2}(y_2')}\,\bar{\phi}_{22}(k_1, k_3, y_2, y_2')\delta(\omega - U_{conv}k_1) e^{-k(y_2+y_2')} dy_2 d$$

(3.11)

Integrating the entire equation over ω, gives:

$$\phi_{pp}(k_1, k_3) = 4\rho_o^2 \int_0^\infty \int_0^\infty \frac{k_1^2}{k^2} \frac{\partial U_1(y_2)}{\partial y_2} \frac{\partial U_1(y_2')}{\partial y_2} \sqrt{\overline{u_2'^2}(y_2)\overline{u_2'^2}(y_2')}\,\bar{\phi}_{22}(k_1, k_3, y_2, y_2') e^{-k(y_2+y_2')} dy_2 dy_2' \tag{3.12}$$

To estimate the wall normalized velocity cross-spectrum, $\bar{\phi}_{22}(k_1, k_3, y_2, y_2')$, we can use the von Kármán (1948) or Leipmann (1951) spectral forms developed for planar wavenumber-frequency spectra developed for homogenous turbulence, in the forms given by Fischer *et al*, 2019 and Grasso *et al*, 2019. Using either of these forms requires computation of integral lengthscale distribution, L_f, for the wall normal velocity fluctuations as a function of y_2 and y_2'. We have

$$\bar{\phi}_{22}(k_1, k_3, y_2, y_2') = \frac{4}{27\pi} \frac{1}{k_e^2} \frac{(k_1/k_e)^2 + (k_3/k_e)^2}{[1 + (k_1/k_e)^2 + (k_3/k_e)^2]^{7/3}}\, \zeta^{7/3} K_{7/3}(\zeta), \tag{3.13}$$

for the von Kármán spectrum, where $\zeta = k_e|y_2 - y_2'|\sqrt{(k_1/k_e)^2 + (k_3/k_e)^2}$, and $k_e = \sqrt{\pi}/L_f\ \Gamma(5/6)/\Gamma(1/3)$ and.

$$\bar{\phi}_{22}(k_1, k_3, y_2, y_2') = \frac{L_f^2}{(2\pi)^{3/2}} \frac{\left(k_1 L_f\right)^2 + \left(k_3 L_f\right)^2}{\left[1 + \left(k_1 L_f\right)^2 + \left(k_3 L_f\right)^2\right]^{5/2}}\, \zeta'^{5/2} K_{5/2}(\zeta') \tag{3.14}$$

$$\zeta' = (|y_2 - y_2'|/L_f)\sqrt{1 + (k_1/k_e)^2 + (k_3/k_e)^2}$$

For the Leipmann spectrum. Note, this formulation includes the dependence of the vertical velocity correlation on both y_2 and y_2', instead of the single coordinate dependence. The estimation of lengthscale, L_f and the wall normal velocity wavenumber-frequency cross-spectrum will be discussed for the wall jet flow studied here as a part of the results section. To obtain the frequency spectrum of the wall pressure, using Taylor's hypothesis,

$$G_{pp}(\omega) = \frac{\int_{-\infty}^{\infty} \phi_{pp}(k_1, k_3) dk_3}{U_c},$$

where, $k_1 \approx K_1 = \omega/U_c$ and U_c is the bulk pressure convection velocity, assumed to be $0.45U_m$ for the wall jet.[Devenport *et al*(2000]

IV. Results and Discussion

Flow Measurements

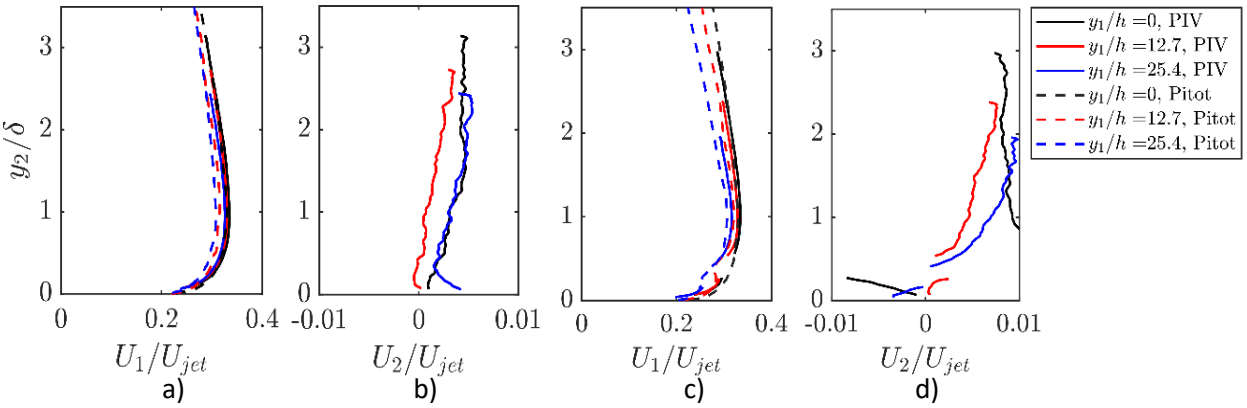

Figure 4 a) Mean streamwise (U_1) and b) wall normal velocity (U_2) profiles normalized over U_{jet}, plotted against the wall normal distance (y_2/δ) for the baseline (without canopy) case. The solid lines represent the data obtained from TR-PIV and the dashed lines correspond to the Pitot measurement data at the same locations. c) Mean streamwise (U_1) and d) wall normal velocity (U_2) profiles normalized over U_{jet}, plotted against the wall normal distance (y_2/δ) for Canopy D placed at a height of 6mm.

Surface pressure measurements in the wall jet were made for nozzle exit velocities ranging from 20 to 50m/s, and are given in detail in Hari *et al*, 2021. Flow measurements using 2D TR-PIV were performed at 30m/s and 50m/s. Figure 4 shows the mean streamwise and wall-normal velocity normalized on maximum velocity in the boundary layer for the baseline (Figs 4 a) and b)) and canopy D at height, $h = 6mm$(Figs 4c) and d)) at three downstream locations corresponding to y_1/h of 0, 12.7 and 25.4. Gonzalez *et al* (2019) and Hari *et al* (2021) observed the surface pressure attenuation at low frequencies (up to 500Hz at U_{jet} of 50m/s), by the canopies is a strong function of the streamwise distance, y_1 normalized over the canopy height, h. The attenuation in this frequency range continues to increase and develop up to y_1/h~15-20 beyond which the peak attenuation is invariant with the change in y_1/h.The three locations chosen here represent the canopy leading edge, region of developing attenuation and region of developed attenuation [Hari *et al*, 2021]. The streamwise mean flow measured using Pitot probe at these locations (dashed lines) have also been compared against the measurements obtained using the PIV (solid lines). The profiles measured using both the techniques are in good agreement within the uncertainty limits of $\pm 0.025\ m/s$ for the Pitot probe measurements and approximately ± 0.5 m/s for PIV measurements at boundary layer height. The PIV captures wall normal distances up to 3.4δ, with the streamwise flow velocity increasing from the wall to the boundary layer thickness and then decreasing beyond to the quiescent air. With the canopy, there is deficit in the mean flow between the rods measured by the Pitot probe, resembling that of a wake profile. The flow below the canopy appears to be slightly slower, while the boundary layer above the canopy is lifted up giving a higher boundary layer height, δ of 16mm compared to the baseline δ of 15mm. The mean vertical velocity in general increases sharply above the canopy, based on momentum conservation. The streamwise mean flow for the baseline and above the canopy seems to fairly scale when normalized by U_{jet}, when plotted against wall normal distance normalized over the boundary layer thickness, δ.

The turbulent stresses in the streamwise, wall-normal direction and the Reynolds shear stress are shown in Fig 5, for the baseline (solid lines) and the canopy D (dashed lines) at height, $h = 6mm$ at 50m/s at three downstream locations. The turbulent stresses when normalized over U_m^2 scales with the wall normal distance normalized over δ. Note that the boundary layer thickness, δ is higher for the canopy than the baseline case and the maximum velocity in the boundary layer, U_m is nearly the same for the baseline and canopy cases. The baseline streamwise and wall –normal turbulence stress normalized by U_{jet}^2 scale well when plotted against wall normal distance normalized over δ. The streamwise turbulence, $\overline{u_1 u_1}$ for the canopy slows a substantial increase in magnitude in the region above the canopy height. The curves are more spread out and do not show a very good collapse on δ and U_{jet}^2. The wall normal velocity

fluctuations, $\overline{u_2 u_2}$, increases slightly in the presence of the canopy, indicating higher vertical turbulence, perhaps due to higher mixing. This is further established by the increase in the Reynolds shear stress indicating a higher mixing in the presence of the canopy. Collapse of the normalized Reynolds stresses appears to be the most unaffected by the canopy. It is slightly negative near the wall indicating, either sweeping or ejection activities occurring closer to the wall and then continues to increase with wall normal distance.

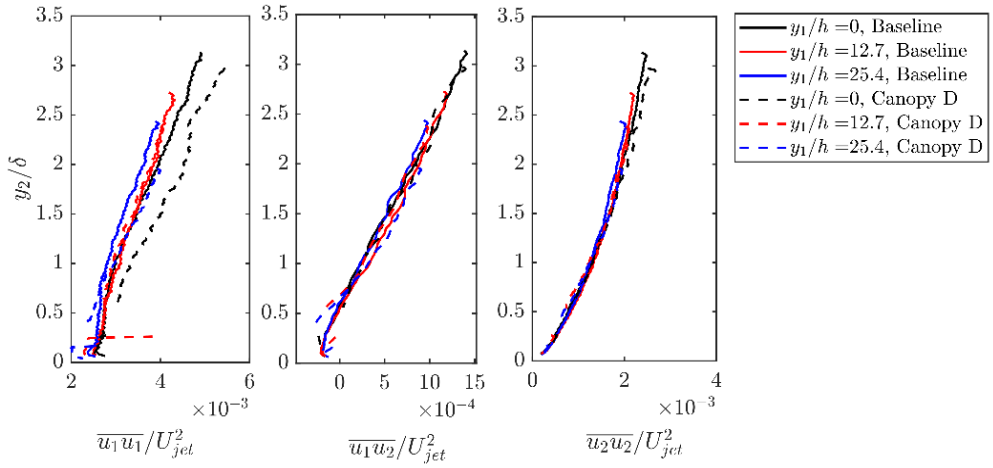

Figure 5: Streamwise turbulent stresses, wall-normal turbulent stresses and the Reynolds shear stresses at three streamwise locations, 0mm, 76.2mm, 152.6mm from the canopy leading edge location for the baseline (solid) and canopy D (dashed) at height, h cases at U_{jet} of 50m/s.

Baseline Case Pressure Prediction (smooth wall, no canopy)

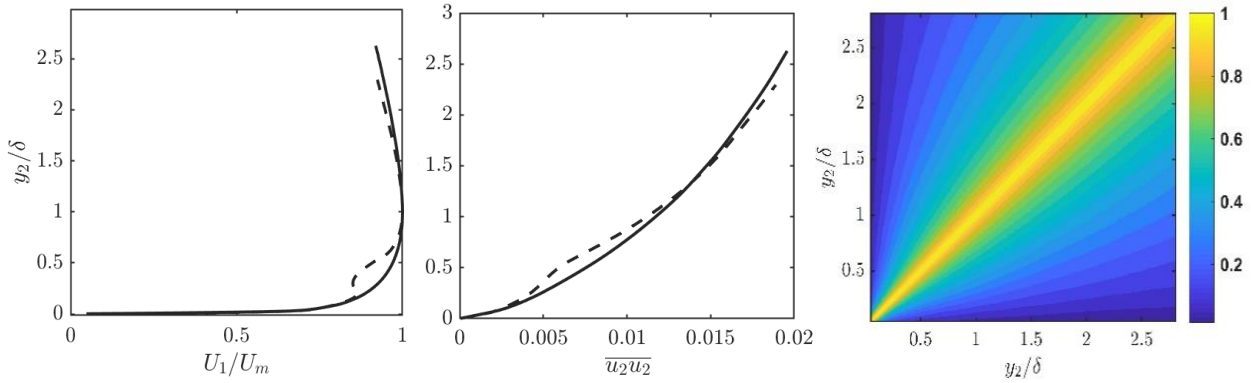

Figure 6: a) Streamwise normalized mean velocity profiles for the baseline and Canopy D cases at U_{jet} of 50m/s and canopy height, h of 6mm. b) Normalized wall-normal turbulent stresses profiles for the baseline and Canopy D c) zero-time delay correlation coefficient of wall normal velocity fluctuations, $R_{22}(y_2, y_2')/[\overline{u_2^2}(y_2)\overline{u_2^2}(y_2')]$ for baseline case obtained experimentally

Computing the rapid term given by Eq. 3.12 requires three derived quantities, the mean velocity gradient, zero-delay wall normal velocity correlation magnitude and the wall normal correlation lengthscale. The mean velocity gradient, dU_1/dy_2, is obtained by taking the numerical differentiation of the measured mean velocity using PIV. The streamwise mean flow measured using the PIV and Pitot probe is in good agreement with the near wall scaling given by George *et al* (2000). Figure 6 shows the mean velocity profile normalized over the maximum boundary layer velocity, plotted as a function of y_2/δ for the baseline case, measured at a streamwise distance, y_1 of 0.1mm from the canopy leading edge. The wall-normal velocity correlations, $\sqrt{\overline{u_2'^2}(y_2)\overline{u_2'^2}(y_2')}$, is computed from the $\sqrt{\overline{u'^2_2}(y_2)}$ obtained from the PIV measurements. Contrary to the conventional turbulent boundary layer, the mean squared fluctuations

continue to increase with wall-normal distance. This is consistent with the presence of significant turbulence mixing in the wall jet up to large wall distances of the order of $y_{1/2}$. The near-wall flow in the wall jet at large Reynolds numbers in previous studies has been shown to be similar to that of a flat-plate boundary layer [Gersten,2015, George *et al*, 2000]. The $\overline{u_2^2}$ profiles need to be interpolated to the near-wall for higher resolution and accuracy, and this has been done using curve-fitting of the experimental measurements performed by DeGraaf and Eaton 2000.

Figure 6c shows normalized zero-delay vertical velocity correlation coefficient, $R_{22}(y_2, y_2')/[\overline{u_2^2}(y_2)\overline{u_2^2}(y_2')]$ as a function of y_2/δ and y_2'/δ for the baseline case from PIV measurements. These are streamwise averaged between distances, y_1 of 0.03m to 0.1m. Highest correlated flow exists along the diagonal with decaying correlations on either side with increasing wall normal separations. The integration of the correlation coefficient with respect to y_2' gives the experimental vertical velocity lengthscale distribution,L_f in the wall normal direction. Since, the normalized vertical velocity wavenumber-frequency spectra, $\bar{\phi}_{22}$ of the experimentally obtained $R_{22}(y_2, y_2')/[\overline{u_2^2}(y_2)\overline{u_2^2}(y_2')]$ does not capture the complete dependency on the streamwise and spanwise wavenumbers, $k_1$and k_3 due to experimental limitations, we estimate $\bar{\phi}_{22}$ for the pressure model using von Kármán spectral form given by Eq 3.15.

Modeling Lengthscale

The integral lengthscale, L_f for the vertical velocity fluctuations in the wall normal direction used in the von Karman model is actually the longitudinal length scale of the hypothetical homogeneous flow used to represent the vertical velocity fluctuation. Experimentally obtained L_f in the inhomogeneous wall-jet flow, shown in Fig 7 is obtained by integrating the $R_{22}(y_2, y_2')$ function (Fig 6c) in the y_2' direction. The lengthscale can be seen to increase with a reducing slope indicating that the eddies are increasing size up to a distance presumably of the order of $y_{1/2}$. This is consistent with our understanding of the wall jet, with two regions of flow, and therefore the presence of an additional mixing layer which lasts much beyond the boundary layer thickness contrary to the conventional turbulent boundary layer flow. Earlier works used Prandtl's mixing layer theory to model integral lengthscales for turbulent boundary layer flows which have been adapted and modified in recent times [Kamruzzaman *et al*, 2011] by including semi-empirical or empirical scaling. Recent work by Grasso *et al*, 2019 employs empirical model by Panton and Linebarger (1974), incorporating Rapid distortion theory formulation. Traditionally this model uses the boundary layer thickness for turbulent boundary layer. However, for the wall jet, we need to consider $y_{1/2}$ to account for the additional mixing layer.

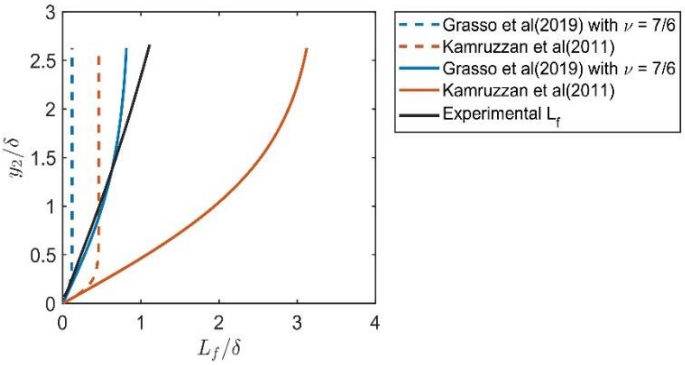

Figure 7: Lengthscale distributions obtained from experimental (black, solid) and empirical formulations in literature. The dashed lines represent the empirical lengthscale using δ as the characteristic normalization length, solid line use $y_{1/2}$ as the length

Figure 7 shows some of the empirical models from literature using both δ and $y_{1/2}$. The formulation given by Grasso *et al* (2019) most closely matches the experimentally obtained lengthscale while the mixing layer formulation used by Kamruzzan *et al* (2011) overpredicts the lengthscale. Since, we are using von Kármán formulation, the length scale must be chosen appropriately to give the closest resemblance to the actual vertical wavenumber spectra, $\bar{\phi}_{22}$.

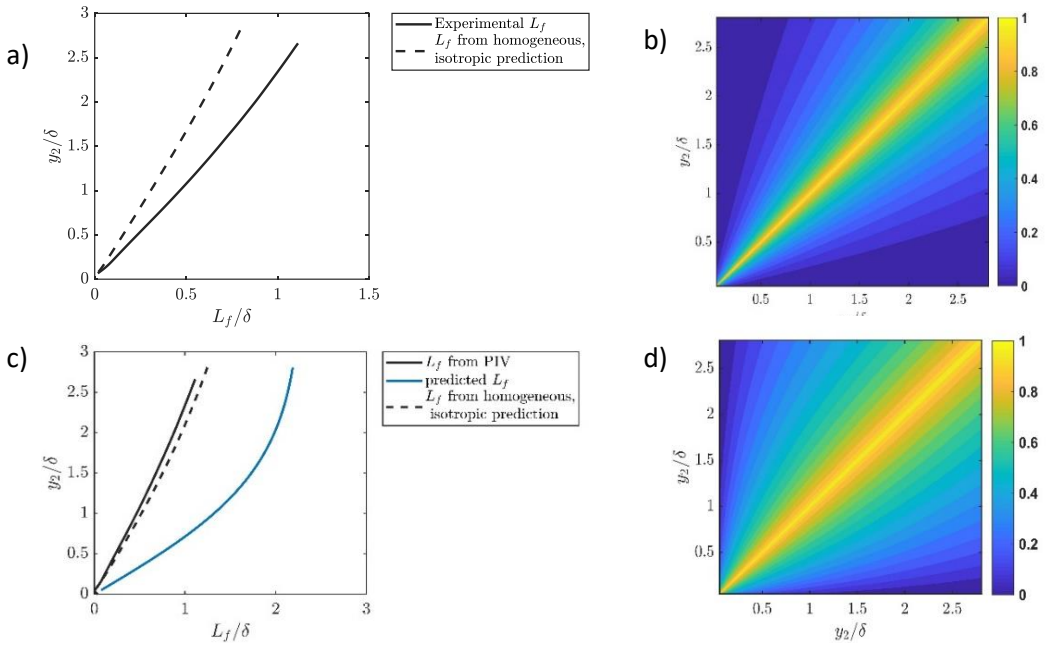

Figure 8 : a) Experimentally obtained lengthscale, L_f(solid) normalized over δ, as a function of the wall normal distance and theoretically obtained L_f (dashed) for an ideal, isotropic and homogeneous flow(von Karman) b) von karman prediction of correlation coefficient implied by experimental L_f.c) predicted lengthscale distribution (blue, solid) and theoretically obtained lengthscale using von Karman formulation. d) vertical velocity correlation coefficient contour implied by predicted L_f given by Eq 3.16

Correlation coefficient, $R_{22}(y_2, y_2')$ contours obtained using von Kármán formulation for experimental lengthscale (Fig 8a and b) is narrower compared to the actual correlation contour (Fig 7c) when the actual measured lengthscale is used for L_f, because of the inhomogeneity. Also, the curvature in the actual correlation map is not accurately captured. A better correlation map is obtained using the model of Panton and Linebarger (1974) ,

$$L_{f_{th}}(y_2) = 0.085 y_{1/2} / 0.41 \tanh(0.41 y_2 / 0.085 y_{1/2}) \tag{3.16}$$

Figure 8 shows the correlation coefficient contour obtained using Eq 3.16, which more closely resembles the experiments. To cross-check, we can integrate the analytic correlation coefficient contour, shown in the Fig 8d, and this matches well with the experimentally obtained L_f (Fig. 8c).

Baseline Surface Pressure Prediction

The rapid term model for the wall jet boundary layer wall pressure fluctuations, obtained using PIV measurements and the lengthscale given by Eq.3.16, is given in Fig 9. The model assumes a pressure convection velocity, U_c of $0.45U_m$ based on wall jet measurements by Devenport *et a l*(2011). The calculation was conducted from a X_2/δ distance of 0.0001 to 2.6 with an uneven spacing of 34 points. The wavenumber domain is divided into logarithmically spaced grids ranging from $k_i\delta$ 0.01 to 20000, where $i = 1{,}3$. Wavenumber convergence was established by running the calculations for higher resolution grids and large range of wavenumbers. Wall pressure predictions are compared with Goody and Howe models for the same boundary layer parameters. Comparison with the experimental data shows the predicted model is much lower than the actual pressure measured, especially at lower frequencies. At very low frequencies, $\omega\delta/U_m < 1$, the pressure prediction closely matches the Howe model (Howe, 1988) for conventional boundary layers. At higher frequencies, $\omega\delta/U_m$>100, the predicted surface spectra matches the Goody model (Goody, 2004) and crosses the experimental pressure spectra. The model appears to have a good resolution in the higher frequency region, therefore, capturing the low wavenumber content effectively. At the lower frequencies, the model fails to capture the high energy content in the mixing layer. We expect the wall jet spectrum to differ from the Goody

and Howe models, specifically at the low frequencies since the flow in the wall jet does not match a canonical zero-pressure gradient turbulent boundary layer.

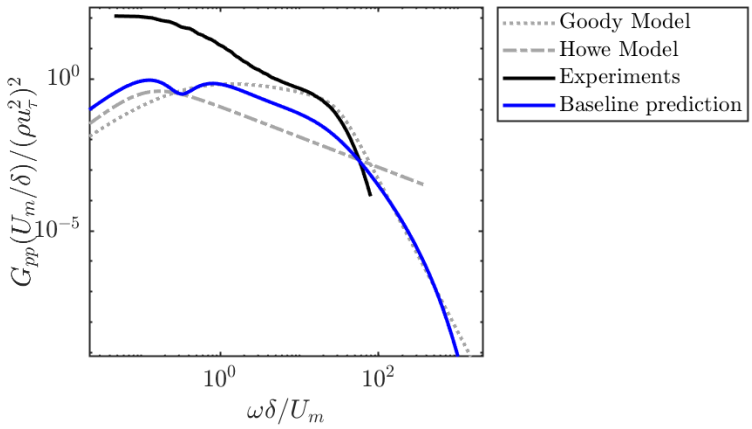

Figure 9: Estimation of the rapid term contribution to the wall pressure spectra for the baseline case(solid, blue) , compared with the experimental data(solid, black), Goody model and Howe model predictions

Effect of Lengthscale

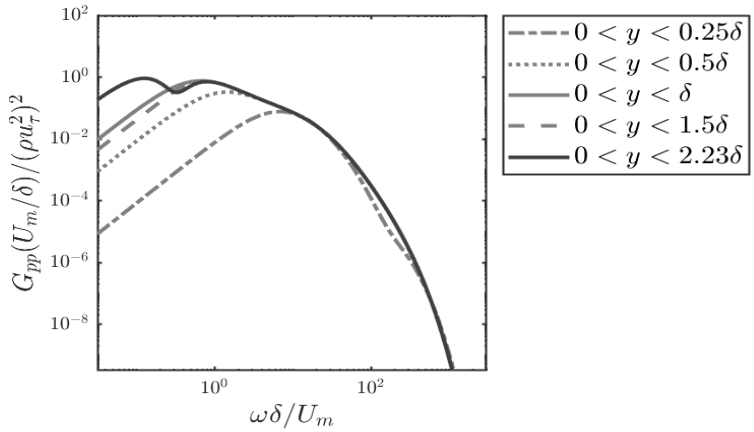

Figure 10: Estimation of the rapid term contribution to the wall pressure spectra for the baseline case for different regions of the wall jet boundary layer flow

Figure 10 shows the rapid term prediction of the wall pressure frequency spectrum determined from Eq 3.12 using a pressure convection velocity of $0.45U_m$ integrated from the wall to different wall normal distances. This plot indicates the contributions of different portions of the boundary layer to the pressure spectrum. We see reduction in the low frequency magnitude of the pressure spectrum as we move closer to the wall, indicating that the near wall boundary layer regions are dominant at higher frequencies, $\omega\delta/U_m > 1$. Up to the boundary layer height, δ, the wall pressure curve is smooth, like a conventional boundary layer frequency pressure spectrum, however, lower in magnitude since we are neglecting the contribution of the outer layer. The model seems to accurately capture the flow within the boundary layer. Moreover, the high frequency region seems to be resolved well and agrees with the Goody model and experiments as seen in Fig 9. Above the boundary layer height, the wall pressure starts to develop a dip.

With increasing wall normal distance, the mean and fluctuating flow quantities reduce in magnitude and their effect on the surface pressure fluctuations reduces. In the case of the wall jet, the mixing layer extending to distances of the order of $y_{1/2}$ plays an important role in the low frequency region [Smith, 2008]. This is captured by the increase in the integral lengthscale of the vertical velocity correlations in the wall normal direction. Adapting two lengthscales for the wall jet flow, $y_{1/2}$ for the outer layer and momentum thickness, θ for the inner layer, proposed by Gonzalez(2019), we observe the surface pressure spectrum is captured accurately and agree with the experiments. The

low frequency pressure spectrum is largely captured by using $y_{1/2}$ as L_f as shown in Fig 11 while the momentum thickness seems to appropriately capturing the high wavenumber content of the pressure spectrum. The high frequency model and experiments also are in good agreement with the Goody model beyond $\omega\delta/U_m > 10$. This tells us that the low frequency energy largely originates from the outer layer of the flow, which consists of the additional mixing layer in case of the wall jet. The outer layer is characterized by large-sized eddies, thus accounting for larger integral lengthscales. Additionally, if we calculate the spectrum using the theoretical lengthscales given in Eq 3.16 as a function of $y_{1/2}$ and θ respectively, then the pressure spectrum, as shown in the Fig 11, closely represents the experiments in magnitude but is unable to capture the dip in the spectrum and the slope of the spectrum at higher frequencies. The constant length scale as opposed to varying lengthscale representing the measured correlations seems to perform better. The varying lengthscale representing the measured correlations is not adequate and perhaps requires the slow term contribution as well to completely predict the surface spectrum. The constant length scales in the two regions, seem to be implicitly accounting for the slow term contribution as well.

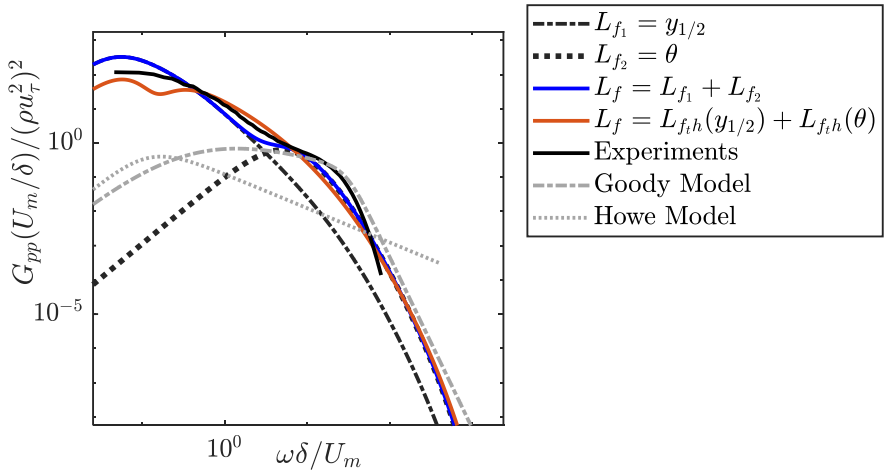

Figure11: Estimation of the rapid term contribution to the wall pressure spectra for the baseline using different lengthscales, $y_{1/2}, \theta$ and sum of the two individual spectra. The predictions are compared with the experiments (solid, black), Goody model and Howe models

Canopy Pressure Spectrum Prediction

Implementation of the rapid term modeling, Eq 3.12 for the surface pressure spectra in the presence of the canopy can be done using the modified mean flow and turbulence profiles. Figure 4 shows the mean flow and the wall normal turbulent stresses for canopy D placed at a height, h of 6mm, measured at a streamwise distance, y_1 of 0.1m from the canopy leading edge location. The wake region between ($y_2/h = 0.5 - 1$), (black, solid line) is not measured by the PIV and at this streamwise location is interpolated using a Gaussian function such that it matches the experimental Pitot measurement data. The boundary layer thickness increases for the canopy compared to the clean wall configuration, therefore reducing the flow velocity below the boundary layer thickness height, δ and causing a slight increase in the flow velocity at distances above δ. The wall normal turbulent stresses in the wake region are obtained by extrapolating the profiles above and below the canopy, available from the PIV measurement. The wake region extrapolation in essence agrees with the turbulent kinetic energy obtained from RANS calculations used for predicting surface pressure spectrum by Gonzalez *et al*(2019). The wake region profiles have been extrapolated to consider spanwise averaged flow below and around the canopy. The lengthscale is modeled using Eq 3.16, which gives a lower lengthscale due to higher δ value for the canopy. This agrees with the reduction obtained in the wall normal velocity correlations and the corresponding reduction in the lengthscale computed from the experiments.

The wall pressure spectrum prediction for the canopy is modified compared to the baseline due to significant changes in the near-wall flow and turbulence. The model predicts reduction in the low frequency pressure spectrum due to canopy, up to frequencies, $\omega\delta/U_m$~20. Comparison with the experiments shows a much lower level of magnitude for both the baseline and the canopy cases, however, note that the model contains contributions largely from the flow

within the wall jet boundary layer. The attenuation in the surface pressure for the rapid term model and the experiments are observed in the same frequency range, $1 < \omega\delta/U_m < 100$. At higher frequencies, the predicted surface pressure for canopies is marginally higher than that of the baseline case, possibly due to higher uncertainty in the near-wall flow below the canopy and the interpolation function used since PIV does not provide data at $y^+ < 50$.

Considering the surface pressure contributions due to flow in regions below and above the canopy separately, neglecting the wake region extrapolation gives a more accurate basis for analysis. Figure 12b shows the frequency wall pressure spectrum predicted by the rapid term modeling for the region below the canopy (blue, dashed) compared with the baseline case (blue, solid line). The canopy reduces the wall pressure fluctuations in the mid-frequency range, however, the model predicts a slight increase in the unsteady pressure at higher frequencies. The pressure spectrum obtained for the region above the canopy largely contributed to frequencies, $\omega\delta/U_m$ less than10. There is reduction in the low frequency pressure spectrum is due to the presence of the canopy, and due to reduction in the length scales. Lifting of the mean flow due to the canopy results in lower mean flow and turbulence near the wall. This appears to be the primary cause of modification to the surface pressure spectra. We also observed that the length scales play a crucial role in determining the lower frequency spectra, while the decay in the wall normal turbulent stresses effect the higher frequency regions.

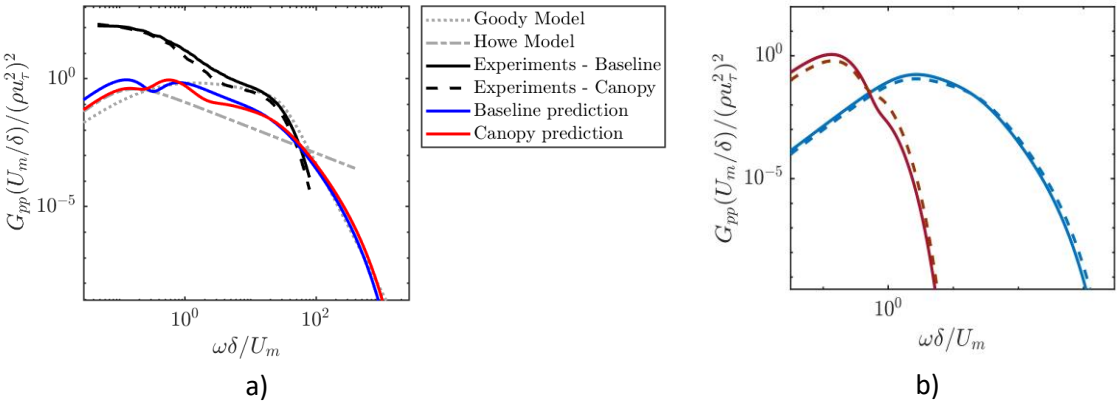

Figure 12: a) Rapid term prediction for flow in the presence of canopy D compared with the baseline prediction. The experimental data for the two cases are also plotted. b) Contributions of regions below(blue) and above(red) the canopy where we have PIV data of the flow, to the rapid term modeling. The solid lines represent the baseline flow case in the same regions and the dashed lines correspond to the canopy case.

V. Conclusion

Wall pressure spectrum prediction was done by developing a model for the rapid source term in the Poisson's equation for a turbulent boundary layer flow. The model was designed using flow data measured using 2D time-resolved PIV in the wall-normal plane capturing the streamwise and wall-normal velocity components. The vertical velocity wavenumber spectrum is modeled by accounting for two-point correlation function. We find that the scale defined by Panton and Linebarger, 1974, when scaled by $y_{1/2}$ works well for the wall jet flow. The correlation coefficient contour map obtained using the von Kàrmàn formulation for this lengthscale matches that obtained experimentally. The model accurately predicts the high frequency pressure spectrum and compares well with the Goody model in this region. The low frequency energy content is not accurately captured due to data availability only up to half the $y_{1/2}$distance, which is roughly the extent of mixing layer region and the size of the largest energy containing turbulent structures. The wall jet flow seems to be characterized largely by two lengthscales, one associated with the flow within the boundary layer or the near-wall flow and the other associated with the outer layer including the mixing layer region. For the canopy, the model predicts reduction in the low and mid frequency pressure fluctuations as observed in the experiments. This model provides an insight into the contribution of changes in the flow on the surface pressure fluctuations. In the future work, this model will be extended to predict the attenuation in surface pressure fluctuations caused by canopies. Additionally measurements with the hot-wire will help establish a better resolution of the streamwise velocity and also permit near-wall measurements.

VI. Acknowledgement

The authors would like to thank the National Science Foundation, in particular Dr. Ron Joslin, for their support of this research under grant CBET-1802915.

References

Afshari, A., Azarpeyvand, M., Dehghan, A. A., and Szoke, M. "Trailing Edge Noise Reduction Using Novel Surface Treatments," *22nd AIAA/CEAS Aeroacoustics Conference*. Lyon, France, 2016

Afshari, A., Azarpeyvand, M., Dehghan, A. A., and Szoke, M. "Effects of Streamwise Surface Treatments on Trailing Edge Noise Reduction," *AIAA Aviation 17*. Denver, CO, 2017

Bertagnolio, Franck, Andreas Fischer, and Wei Jun Zhu. "Tuning of turbulent boundary layer anisotropy for improved surface pressure and trailing-edge noise modeling." *Journal of Sound and Vibration* 333.3 (2014): 991-1010.

Blake, William K. *Mechanics of flow-induced sound and vibration, Volume 2: Complex flow-structure interactions*. Academic press, 2017.

Bodling, A., Agrawal, B. R., Sharma, A., Clark, I., Alexander, W. N., and Devenport, W. J. "Numerical Investigations of Bio-Inspired Blade Designs to Reduce Broadband Noise in Aircraft Engines and Wind Turbines," *55th AIAA Aerospace Sciences Meeting*. Grapevine, TX, 2017.

Bull, M. K. "Wall-pressure fluctuations associated with subsonic turbulent boundary layer flow." *Journal of Fluid Mechanics* 28.4 (1967): 719-754.

Chase, David M. "Modeling the wavevector-frequency spectrum of turbulent boundary layer wall pressure." *Journal of sound and Vibration* 70.1 (1980): 29-67.

Chang III, Peter A., Ugo Piomelli, and William K. Blake. "Relationship between wall pressure and velocity-field sources." *Physics of Fluids* 11.11 (1999): 3434-3448.

Clark, I. A., Daly, C. A., Devenport, W., Alexander, W. N., Peake, N., Jaworski, J. W., and Glegg, S. "Bio-inspired canopies for the reduction of roughness noise," *Journal of Sound and Vibration* Vol. 385, 2016, pp. 33-54.

Clark, I. A., Alexander, W. N., Devenport, W., Glegg, S., Jaworski, J. W., Daly, C., and Peake, N. "Bioinspired Trailing-Edge Noise Control," *AIAA Journal* Vol. 55, No. 3, 2017, pp. 740-754

Corcos, G. M. "The structure of the turbulent pressure field in boundary-layer flows." *Journal of Fluid Mechanics* 18.3 (1964): 353-378.

De Graaff, David B., and John K. Eaton. "Reynolds-number scaling of the flat-plate turbulent boundary layer." *Journal of Fluid Mechanics* 422 (2000): 319-346.

Farabee, Theodore M., and Mario J. Casarella. "Spectral features of wall pressure fluctuations beneath turbulent boundary layers." *Physics of Fluids A: Fluid Dynamics* 3.10 (1991): 2410-2420.

George, William K., et al. "A similarity theory for the turbulent plane wall jet without external stream." *Journal of Fluid Mechanics* 425 (2000): 367-411.

Gersten, Klaus. "The asymptotic downstream flow of plane turbulent wall jets without external stream." *Journal of Fluid Mechanics* 779 (2015): 351.

Glegg, Stewart, and William Devenport. *Aeroacoustics of low Mach number flows: fundamentals, analysis, and measurement*. Academic Press, 2017.

Gonzalez, A., Glegg, S. A., Hari, N., & Devenport, W. J. (2019). Fundamental Studies of the Mechanisms of Pressure Shielding. In *25th AIAA/CEAS Aeroacoustics Conference* (p. 2403).

Gonzalez, A. (2019). A Computational Analysis of Bio-Inspired Modified Boundary Layers for Acoustic Pressure Shielding in A Turbulent Wall Jet. MS, Florida Atlantic University

Goody, Michael. "Empirical spectral model of surface pressure fluctuations." *AIAA journal* 42.9 (2004): 1788-1794.

Grasso, Gabriele, et al. "Analytical models of the wall-pressure spectrum under a turbulent boundary layer with adverse pressure gradient." *Journal of Fluid Mechanics* 877 (2019): 1007-1062.

Nurani Hari, N., Szoke, M., Devenport, W. J., & Glegg, S. A. (2021). Understanding Pressure Shielding by Canopies. In *AIAA Scitech 2021 Forum* (p. 0817).

Howe, M. S.. *"The turbulent boundary-layer rough-wall pressure spectrum at acoustic and subconvective wavenumbers*." Proceedings of the Royal Society of London. A. Mathematical and Physical Sciences 415 (1988): 141 - 161.

Jaiswal, Prateek, et al. "On the use of two-point velocity correlation in wall-pressure models for turbulent flow past a trailing edge under adverse pressure gradient." *Physics of Fluids* 32.10 (2020): 105105.

Kamruzzaman, Mohammad, et al. "On the length scales of turbulence for aeroacoustic applications." *17th AIAA/CEAS Aeroacoustics Conference (32nd AIAA Aeroacoustics Conference)*. 2011.

Kleinfelter, A. W., Repasky, R., Hari, N., Letica, S., Vishwanathan, V., Organski, L., ... & Devenport, W. J. (2019). Development and Calibration of a new Anechoic Wall Jet Wind Tunnel. In *AIAA Scitech 2019 Forum* (p. 1936).

Kraichnan, Robert H. "Pressure fluctuations in turbulent flow over a flat plate." *The Journal of the Acoustical Society of America* 28.3 (1956): 378-390.

Liepmann, Hans Wolfgang, John Laufer, and Kate Liepmann. "On the spectrum of isotropic turbulence." (1951).

Lilley, G. "A study of the silent flight of the owl," 1998.

Millican, A. J., Clark, I., Devenport, W. J., and Alexander, W. N. "Owl-Inspired Trailing Edge Noise Treatments: Acoustic and Flow Measurements," *55th AIAA Aerospace Sciences Meeting*. Grapevine TX, 2017.

Nurani Hari, N., Szoke, M., Devenport, W. J., & Glegg, S. A. (2021). Understanding Pressure Shielding by Canopies. In *AIAA Scitech 2021 Forum* (p. 0817)

Panton, Ronald L., and John H. Linebarger. "Wall pressure spectra calculations for equilibrium boundary layers." (1974).

Slama, Myriam, Cédric Leblond, and Pierre Sagaut. "A Kriging-based elliptic extended anisotropic model for the turbulent boundary layer wall pressure spectrum." *Journal of Fluid Mechanics* 840 (2018): 25-55.

Smith, Benjamin S., "Wall jet Boundary Layer Flows Over Smooth and Rough Surfaces", PhD Disseration, 2008

Devenport, W. J., Grissom, D. L., Alexander, W. N., Smith, B. S., & Glegg, S. A. (2011). Measurements of roughness noise. *Journal of Sound and Vibration*, *330*(17), 4250-4273.

Von Karman, Theodore. "Progress in the statistical theory of turbulence." *Proceedings of the National Academy of Sciences of the United States of America* 34.11 (1948): 530.

Willmarth, W. W., and F. W. Roos. "Resolution and structure of the wall pressure field beneath a turbulent boundary layer." *Journal of Fluid Mechanics* 22.1 (1965): 81-94.

Wygnanski, I., Katz, Y., & Horev, E. (1992). On the applicability of various scaling laws to the turbulent wall jet. *Journal of Fluid Mechanics*, *234*, 669-690